IEEE Access
Multidisciplinary : Rapid Review : Open Access Journal

Received August 2, 2018, accepted September 6, 2018, date of publication September 24, 2018, date of current version October 19, 2018.

Digital Object Identifier 10.1109/ACCESS.2018.2871730

FPGA Implementation of Sensorless Sliding Mode Observer With a Novel Rotation Direction Detection for PMSM Drives

ZHIXUN MA[1,2], (Member, IEEE), AND XIN ZHANG[2], (Member, IEEE)
[1]National Maglev Transportation Engineering R&D Center, Tongji University, Shanghai 201804, China
[2]School of Electrical and Electronic Engineering, Nanyang Technological University, Singapore 639798

Corresponding author: Xin Zhang (jackzhang@ntu.edu.sg)

This work was supported by the NTU-SUG Funding: Stability, Reliability and Advanced Control of Power Electronic Systems (SCOPES).

ABSTRACT This paper proposes an field programmable gate array (FPGA) implementation of a sensorless controller for surface mounted permanent magnet synchronous machines. Position and speed are both estimated by a sliding mode observer (SMO) which is based on the PMSM stator frame model. The sliding mode manifold is chosen on the real stator current trajetory. In the SMO, a sign function of current error in the feedback correction is adopted. The estimated speed and position are realized on an FPGA controller by COordinate Rotation Digital Computer (CORDIC) algorithm. Using model-based design, with the tools of MATLAB/Simulink and hardware description language coder, the whole control system is designed and implemented in a single FPGA chip. Dedicated hardware optimization algorithms such as pipeline and resource sharing are developed for the implementation as well. The sign function is realized by fully hardware with a relatively high switching frequency. Meanwhile, a fast and practical rotation direction detection method which is based on back electromotive force information is proposed. Experimental results show that the proposed FPGA implemented sensorless SMO for PMSM drives is robust and has high performance.

INDEX TERMS Sensorless control, sliding mode observer (SMO), permanent magnet synchronous machine (PMSM), FPGA (field programmable gate array).

I. INTRODUCTION

Permanent Magnet Synchronous Machines (PMSMs) are used more and more widely in industrial electrical drive systems in recent years due to their advantages, such as high efficiency, high power density and high torque-to-weight-ratio. In the high performance PMSM drive systems, position sensors are required for detecting the rotor position. Unfortunately, these position sensors are not desired to be used in industrial applications because their existence has several disadvantages for the drive systems. For example, the position sensors are difficult to be mounted on the shaft of the PMSMs and require extra wires, meanwhile, increase the system cost, etc. Therefore, removing these position sensors is desirable and methods for this purpose are usually called ‘‘sensorless’’ (or ‘‘encoderless’’, ‘‘self-sensing’’, etc.).

Sensorless control for PMSM drives has been extensively investigated for three decades. At present, the existing sensorless control methods mainly belong to two categories. The first one is saliency tracking based method. The other is fundamental model based method. Saliency tracking based method is the only method that can work at standstill and in the very low speed range. Generally, this category method can be further divided into two groups: continuous high frequency (HF) injection and transient excitation methods. The well-known rotating HF injection [1] and alternating HF injection methods [2], [3] both belong to continuous HF injection group. Although the working performance of all the HF injection methods are relatively good and attractive, signal injection could cause extra losses, torque ripple and transient disturbances. In the transient excitation category, there are INFORM (Indirect Flux detection by Online Reactance Measurement) method [4]– [8], fundamental PWM excitation method and arbitrary injection method, etc. These methods are usually required to modify the hardware of the drive systems, which are not desirable and also difficult to be implemented in industrial applications.

According to state of the art techniques, saliency tracking based methods either need the PMSM saliency information or have interference of drive systems in hardware or in control performance. Hence, fundamental model based

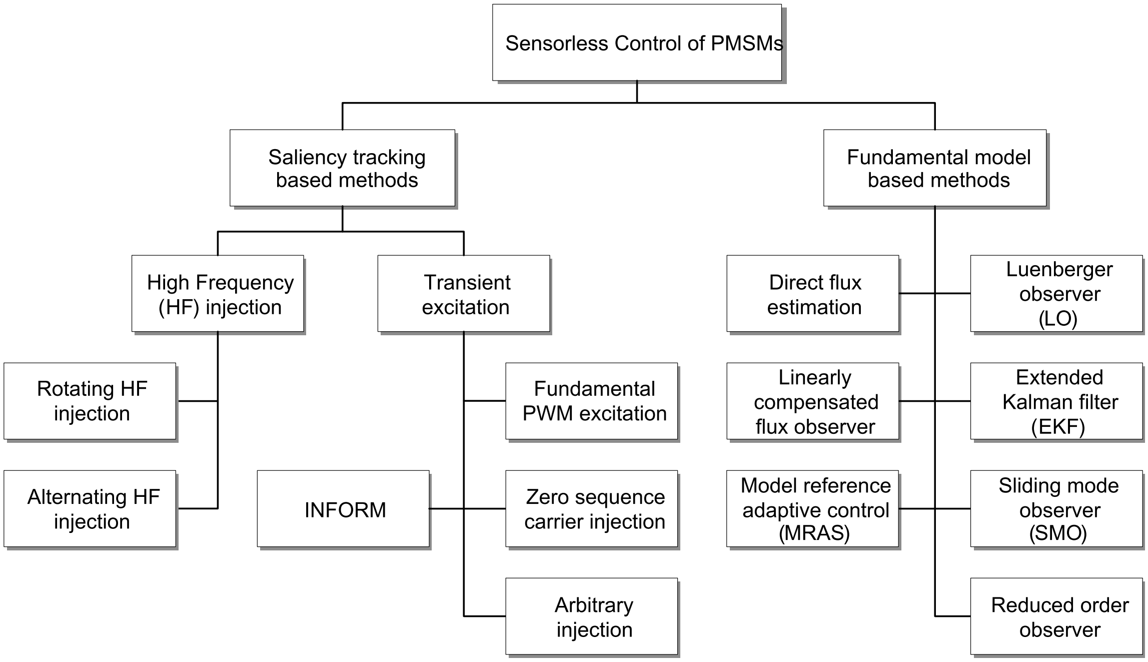

FIGURE 1. Classification of sensorless control methods for PMSM drives.

methods are still received more and more attention. A great amount of works are trying to improve the low speed performance or to use hybrid control methods in this research direction [9], [10]. The back electromotive force (EMF) based observer has advantages of simplicity and straightforwardness [9], [11]. In this category, there are a large number of various state observer based methods for position estimation, such as Luenberger observer (LO), sliding mode observer (SMO), extended Kalman filter (EKF), and model reference adaptive system (MRAS), etc [12]– [16]. Sensorless SMO has been widely investigated in rotor position and speed estimation for PMSM drives [17], [18]. However, there are still many problems to be solved or improved, such as initial position estimation, parameter sensitivity, and especially FPGA implementation. The classification of sensorless control approaches for PMSM drives is summarized in Figure 1.

Nowadays, compared with microcontrollers or DSPs, field programmable gate arrays (FPGAs) have some advantages for drive control. For instance, parallel processing capabilities can shorten the computational time to a large extent, which results in a lower control delay and better dynamic performance of the drive system; all dedicated interfaces and control algorithms can be implemented in a single chip, which is flexible and friendly to PCB design. Hence, FPGAs are becoming more and more popular as control platforms for electrical drives [19]– [22]. In this work, an FPGA implementation method of the SMO for sensorless PMSM drives is proposed. Using model based design, the whole control algorithm including field oriented control (FOC) and sensorless SMO is implemented in a low cost FPGA chip. Pipeline and resource sharing optimization methods as well as the CORDIC (COordinate Rotation Digital Computer) algorithm are adopted in the design. In the implementation of SMO algorithm, a fast rotation direction detection method is proposed which ensures the robustness of sensorless SMO. The rest part of this paper is organized as follows: mathematical model of PMSM is presented in Section II; In Section III, position observer based on SMO is described; Section IV elaborates proposed FPGA implementation method; After experimental results in Section V, Section VI concludes this work.

II. MATHEMATICAL MODEL OF A PMSM

In this work, only a simplified mathematical model of a PMSM is considered. This means that magnetic saturation is neglected. The stator voltage is composed of two parts. One part is the resistance loss, and the other part can be seen as back electromotive force (EMF) which depends on the rate of change of the stator flux linkage. So, the stator voltage equation of a PMSM in cartesian stator coordinates (α, β) can be described as follows

$$\boldsymbol{u}_s^s = R_s \boldsymbol{i}_s^s + \frac{d\boldsymbol{\psi}_s^s}{dt}. \tag{1}$$

Where $\boldsymbol{u}_s^s = [u_\alpha, u_\beta]^T$ and $\boldsymbol{i}_s = [i_\alpha, i_\beta]^T$ are the stator voltage and current, respectively. R_s is the stator resistance. $\boldsymbol{\psi}_s^s$ is the stator flux linkage.

The stator flux linkage could be assumed to be caused by the stator current and the rotor magnetization together, that is

$$\boldsymbol{\psi}_s^s = \mathbf{L}_s^s \boldsymbol{i}_s^s + \boldsymbol{\psi}_{pm}^s \tag{2}$$

The calculation of rotor flux linkage $\boldsymbol{\psi}_{pm}^s$ in the stator frame is the transformation from its rotor frame value $\boldsymbol{\psi}_{pm}^{r}$.

$$\boldsymbol{\psi}_{pm}^{s} = \mathbf{T}\boldsymbol{\psi}_{pm}^{r} = \begin{bmatrix} \cos\theta & -\sin\theta \\ \sin\theta & \cos\theta \end{bmatrix} \begin{bmatrix} \Psi_{pm} \\ 0 \end{bmatrix} \tag{3}$$

where θ is the rotor position angle, $\mathbf{T}$ is the transformation matrix and Ψ_{pm} is the magnitude of the rotor flux linkage. The inductance tensor $\mathbf{L}_s^s$ can also be transformed from its rotor coordinate value $\mathbf{L}_s^r$

$$\mathbf{L}_s^s = \mathbf{T}\mathbf{L}_s^r\mathbf{T}^{-1} = \mathbf{T}\begin{bmatrix} L_d & 0 \\ 0 & L_q \end{bmatrix}\mathbf{T}^{-1} \tag{4}$$

where L_d, L_q are the d-axis and q-axis inductances respectively. $\mathbf{T}^{-1}$ is the inverse matrix of $\mathbf{T}$.

In the rotor reference frame, the stator voltage and stator flux linkage can be described as

$$\boldsymbol{u}_s^r = R_s\boldsymbol{i}_s^r + \frac{d\boldsymbol{\psi}_s^r}{dt} + \omega_r\mathbf{O}\boldsymbol{\psi}_s^r. \tag{5}$$

$$\boldsymbol{\psi}_s^r = \mathbf{L}_s^r\boldsymbol{i}_s^r + \boldsymbol{\psi}_{pm}^r. \tag{6}$$

Where $\boldsymbol{u}_s^r = [u_d, u_q]^T$, $\boldsymbol{\psi}_s^r = [\psi_d, \psi_q]^T$, and $\boldsymbol{i}_s^r = [i_d, i_q]^T$. ω_r is the electrical speed (in rad/sec). In analogy to the complex notation, the positive $\pi/2$ rotation is defined as matrix $\mathbf{O}$

$$\mathbf{O} = \begin{bmatrix} 0 & -1 \\ 1 & 0 \end{bmatrix}. \tag{7}$$

The useful relationships between these matrices are

$$\mathbf{TO} = \mathbf{OT}. \tag{8}$$

The torque produced by a PMSM can be calculated mathematically by the vector product of the stator current and stator flux linkage in the stationary reference frame by (9) or in the rotating reference frame by (10).

$$T_m = \frac{3}{2}p\boldsymbol{i}_s^{sT}\mathbf{O}\boldsymbol{\psi}_s^s = \frac{3}{2}p(\psi_\alpha i_\alpha - \psi_\beta i_\beta). \tag{9}$$

$$T_m = \frac{3}{2}p\boldsymbol{i}_s^{rT}\mathbf{O}\boldsymbol{\psi}_s^r = \frac{3}{2}p(\psi_d i_q - \psi_q i_d). \tag{10}$$

Where p is the number of pole pairs of the PMSM, $\boldsymbol{\psi}_s^s = [\psi_\alpha, \psi_\beta]^T$ is the stator flux linkage. The factor $\frac{3}{2}$ demonstrates that the used transformation is non-power invariant. It must be used whenever energy or power quantities are computed using transformation of voltages and/or currents.

The equation used to model the dynamics is given by (11), where J_m is the system inertia and B_m is the system friction coefficient. Equation (12) presents that the electrical speed ω_r (in rad/sec) is related to the mechanical speed ω_m by the number of pole pairs p.

$$J_m\frac{d\omega_m}{dt} = T_m - T_l - B_m\omega_m \tag{11}$$

$$\omega_r = p\omega_m \tag{12}$$

III. SENSORLESS CONTROL USING A SLIDING MODE OBSERVER

A. FUNDAMENTALS OF THE SLIDING MODE CONTROL

Here a nonlinear time-invariant system is considered, and its state space model can be described as

$$\begin{aligned} \dot{\boldsymbol{x}} &= \boldsymbol{f}(\boldsymbol{x}) + \mathbf{B}(\boldsymbol{x})\boldsymbol{u} + z(\boldsymbol{x}) \\ &= \boldsymbol{f}(\boldsymbol{x}) + \sum_{i=1}^{m}\boldsymbol{b}_i(\boldsymbol{x})u_i + z(\boldsymbol{x}) \quad \text{with } \boldsymbol{x}(t_0) = \boldsymbol{x}_0, \end{aligned} \tag{13}$$

where $\boldsymbol{x} \in \mathbb{R}^n$ is the system state and $\boldsymbol{u} \in \mathbb{R}^m$ is the control input. The vector functions $\boldsymbol{f}, \boldsymbol{b} : \mathbb{R}^n \mapsto \mathbb{R}^n$ and the matrix $\mathbf{B} = (\boldsymbol{b}_1\boldsymbol{b}_2 \ldots \boldsymbol{b}_m)$ are assumed to be continuously differentiable. The vector function $z : \mathbb{R}^n \mapsto \mathbb{R}^n$ summarizes the external disturbances and unknown parameter uncertainties.

It is assumed that $z(\boldsymbol{x})$ satisfies the following condition for each $\boldsymbol{x}$,

$$z(\boldsymbol{x}) \in span\{\mathbf{B}(\boldsymbol{x})\}. \tag{14}$$

Therefore, there exists a control input $\boldsymbol{u}$, which makes $\mathbf{B}(\boldsymbol{x})\boldsymbol{u} = -z(\boldsymbol{x})$, i.e. the system is invariant to the uncertainties and disturbances $z(\boldsymbol{x})$. The sliding mode control theory handles state-feedback control schemes which utilizes switching-control actions. Accordingly, a discontinuous function of the system state is selected as the control input $\boldsymbol{u}(\boldsymbol{x})$

$$\boldsymbol{u}(\boldsymbol{x}) = \begin{cases} \boldsymbol{u}^+(\boldsymbol{x}) & \text{for } s(\boldsymbol{x}) > 0 \\ \boldsymbol{u}^-(\boldsymbol{x}) & \text{for } s(\boldsymbol{x}) < 0. \end{cases} \tag{15}$$

Where $\boldsymbol{s} : \mathbb{R}^n \mapsto \mathbb{R}^m$ is a continuously differentiable function. The feedback signal $\boldsymbol{u}(\boldsymbol{x})$ exhibits a point of discontinuity at $s(\boldsymbol{x}) = 0$;

$$\lim_{s(\boldsymbol{x})\to 0}\boldsymbol{u}^+(\boldsymbol{x}) \neq \lim_{s(\boldsymbol{x})\to 0}\boldsymbol{u}^-(\boldsymbol{x})$$

and is not a continuous function of time [23].

B. SLIDING MODE OBSERVER

Since the normally measured value of the standard drive systems is just only the current, the stator current is usually selected for the sliding mode observer to estimate the position and speed of the PMSM drives with discontinuous control. $s(\boldsymbol{x}) = 0$ is selected as the sliding mode manifold on the actual stator current trajectory. As a result, if the estimated currents arrive the manifold, it will be enforced in the manifold in system spaces and the sliding mode will be appeared. Therefore, the estimated currents can track the real ones free from the disturbances and uncertainties which means the estimation error of the current becomes zero [13], [24].

1) DESIGN OF THE SLIDING MODE OBSERVER

Considering the PMSM model in the stator reference frame as presented in Section II. Here, it is written again for a convenient form.

$$\frac{d\boldsymbol{i}_s^s}{dt} = -\mathbf{L}_s^{-1}R_s\boldsymbol{i}_s^s + \mathbf{L}_s^{-1}(\boldsymbol{u}_s^s - \boldsymbol{e}_s^s). \tag{16}$$

Where $\boldsymbol{i}_s^s = [i_\alpha, i_\beta]^T$ is the stator current, $\boldsymbol{u}_s^s = [u_\alpha, u_\beta]^T$ is the stator voltage, $\boldsymbol{e}_s^s = [e_\alpha, e_\beta]^T = \omega\Psi_{pm}[-\sin\theta, \cos\theta]^T$ is the back electromotive force (EMF), $\mathbf{L}_s = \begin{bmatrix} L_s & 0 \\ 0 & L_s \end{bmatrix}$ is the stator inductance matrix.(Here, the machine is supposed to be a SMPMSM.) R_s and L_s are the stator resistance and inductance, respectively.

The sliding mode observer is designed according to the SMPMSM model,

$$\frac{d\hat{\boldsymbol{i}}_s^s}{dt} = -\mathbf{L}_s^{-1}R_s\hat{\boldsymbol{i}}_s^s + \mathbf{L}_s^{-1}(\boldsymbol{u}_s^s - \boldsymbol{z}_s^s), \tag{17}$$

$$\boldsymbol{z}_s^s = k_{sw} \cdot sign(\hat{\boldsymbol{i}}_s^s - \boldsymbol{i}_s^s) = k_{sw} \cdot \begin{bmatrix} sign(\hat{i}_\alpha - i_\alpha) \\ sign(\hat{i}_\beta - i_\beta) \end{bmatrix}. \tag{18}$$

Where k_{sw} is the switching gain of the discontinuous control $\boldsymbol{z}_s^s$, which is normally positive, i.e. $k_{sw} > 0$. The values with hat indicate they are estimated variables. The current estimation error is defined as $\bar{\boldsymbol{i}}_s^s = \hat{\boldsymbol{i}}_s^s - \boldsymbol{i}_s^s$.

2) STABILITY ANALYSIS OF THE SLIDING MODE OBSERVER

The sliding mode surface can be defined as follows

$$\boldsymbol{s} = [s_\alpha, s_\beta]^T = [\hat{i}_\alpha - i_\alpha, \hat{i}_\beta - i_\beta]^T, \tag{19}$$

where $s_\alpha = \bar{i}_\alpha$, and $s_\beta = \bar{i}_\beta$.

If the estimation errors are located on the sliding surface, the estimation errors become zero, i.e., $\hat{i}_\alpha = i_\alpha$ and $\hat{i}_\beta = i_\beta$. At this moment, the sliding surface is $\boldsymbol{s} = 0$ and the observer is robust against the system disturbances and uncertainties.

The gain of the sensorless sliding mode observer can be determined by the Lyapunov second criterion via estimating the stability of this observer. Make the positive definite function

$$V = \frac{1}{2}\boldsymbol{s}^T\boldsymbol{s} \tag{20}$$

be a Lyapunov function's candidate. The prerequisite of the stable sliding mode is $\dot{V} < 0$. The derivative of V is

$$\dot{V} = \boldsymbol{s}^T\dot{\boldsymbol{s}}. \tag{21}$$

By the equation (17), the derivative of $\boldsymbol{s}$ can be presented as

$$\dot{\boldsymbol{s}} = \begin{bmatrix} \dot{s}_\alpha \\ \dot{s}_\beta \end{bmatrix} = \begin{bmatrix} \frac{R_s}{L_s}\bar{i}_\alpha + \frac{1}{L_s}(e_\alpha - k_{sw} \cdot sign(\bar{i}_\alpha)) \\ \frac{R_s}{L_s}\bar{i}_\beta + \frac{1}{L_s}(e_\beta - k_{sw} \cdot sign(\bar{i}_\beta)) \end{bmatrix}. \tag{22}$$

Substitute equation (22) into equation (21), Then the precondition of the stability is

$$\dot{V} = \begin{bmatrix} \bar{i}_\alpha \\ \bar{i}_\beta \end{bmatrix}^T \begin{bmatrix} \frac{R_s}{L_s}\bar{i}_\alpha + \frac{1}{L_s}(e_\alpha - k_{sw} \cdot sign(\bar{i}_\alpha)) \\ \frac{R_s}{L_s}\bar{i}_\beta + \frac{1}{L_s}(e_\beta - k_{sw} \cdot sign(\bar{i}_\beta)) \end{bmatrix} < 0. \tag{23}$$

To satisfy the condition $\dot{V} < 0$, the equation (23) is decomposed into two equations as follows

$$\begin{bmatrix} \bar{i}_\alpha \\ \bar{i}_\beta \end{bmatrix}^T \begin{bmatrix} \frac{R_s}{L_s}\bar{i}_\alpha \\ \frac{R_s}{L_s}\bar{i}_\beta \end{bmatrix} = 0, \tag{24}$$

$$\begin{bmatrix} \bar{i}_\alpha \\ \bar{i}_\beta \end{bmatrix}^T \begin{bmatrix} \frac{1}{L_s}(e_\alpha - k_{sw} \cdot sign(\bar{i}_\alpha)) \\ \frac{1}{L_s}(e_\beta - k_{sw} \cdot sign(\bar{i}_\beta)) \end{bmatrix} < 0. \tag{25}$$

In order to keep the observer stable, the observer gains should satisfy equation (25). Therefore, the observer gain can be derived to satisfy the inequality condition as

$$k_{sw} \geq max(|e_\alpha|, |e_\beta|). \tag{26}$$

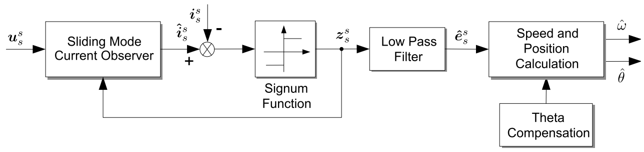

FIGURE 2. Block diagram of sensorless control using SMO.

3) POSITION ESTIMATION USING SLIDING MODE OBSERVER

The sensorless sliding mode observer used for position estimation is presented in Figure 2, where the signum function is selected as the switching function and the low-pass filter (LPF) is used for eliminating the chattering problem generated by the switching. The following equation describes the estimated back EMF

$$\hat{\boldsymbol{e}}_s^s = \frac{\omega_c}{s + \omega_c}\boldsymbol{z}_s^s \tag{27}$$

where, ω_c is the LPF cut-off frequency and it needs to be selected properly to extract the signal of the position and to remove the high frequency component. Hence, it is desirable to have large difference between the switching frequency and the fundamental frequency. In this case, it is much flexible to choose the ω_c, and the tracking of the stator currents performance will be better.

Using the estimated back EMF, the position and velocity of the rotor are calculated from

$$\hat{\theta}_e = -\arctan(\frac{\hat{e}_\alpha}{\hat{e}_\beta}) \tag{28}$$

$$\hat{\omega} = \frac{d\hat{\theta}}{dt}. \tag{29}$$

The phase lag will be un-avoidably introduced by the LPF which is utilized to eliminate the chattering effects. In addition, the relationship between the phase lag and the phase response of the LPF is very clear: a lower cut-off frequency also means a greater phase lag. Therefore, the phase lag compensation becomes necessary for the phase response of the LPF, whose compensation value can be derived by the equation (30). Here, ω is the speed of the machine.

$$\Delta\theta = \arctan(\frac{\omega}{\omega_c}). \tag{30}$$

Finally, the estimated rotor position is obtained

$$\hat{\theta} = \hat{\theta}_e + \Delta\theta. \tag{31}$$

IV. FPGA IMPLEMENTATION OF SENSORLESS SMO OF A PMSM

A. MODEL-BASED DESIGN PROCESS

The typical design flow for conventional FPGA implementation can be described as: firstly a simulation model is created, then register transfer logic is manually written in hardware description language (HDL), at last, the program is synthesized and a bit stream is created from it. Actually, it is very time consuming. Model-based design (MBD) can save cost and time by verifying functionality and tuning system performance prior to logic design. Moreover, it is very proper for complex control algorithm design and implementation compared with traditional design method.

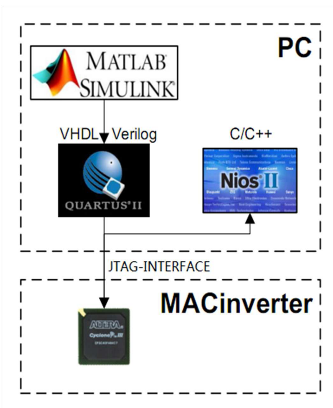

FIGURE 3. Tools and Design flow for FPGA implementation.

Figure 3 presents the model-based design flow and tools used in this work. First, the continuous control algorithm is modelled and verified in MATLAB/Simulink. In this process, the algorithm validation is done. Next, the continuous model is discretized and transferred to corresponding discrete model with the fixed point data type. In addition, hardware implementation optimal algorithms are designed in this step, such as pipeline and resource sharing. It can be seen that the register transfer level simulation for control algorithm which is going to be implemented in FPGA is prepared in MATLAB/Simulink. After this process, HDL code is then generated automatically from the discrete fixed point model by MATLAB toolboxes. Finally, the corresponding HDL code is synthesized, placed and routed with Altera Quartus II software. In this work, a low cost Altera Cyclone III FPGA EP3C40F484C7 is used for implementation of control algorithms.

B. FPGA IMPLEMENTATION DESCRIBTION

The block diagram of sensorless control for PMSM drives based on SMO is presented in Figure 4.

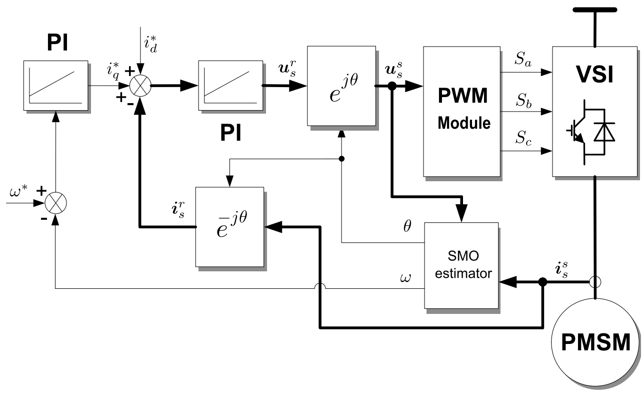

FIGURE 4. Sensorless control of PMSM based on SMO.

Figure 5 presents the developed architecture for an FPGA-based implementation of FOC for PMSM drives. The architecture is divided into different reusable modules. In the top level, there are: 1) time control module; 2) data acquisition interface module; 3) current control module; 4) data transfer Avalon bus interface; and 5) NIOS II processor. The function of the time control module is to control the time sequence of all the modules. In the data acquisition interface module, the decimation filter, which is the digital part of the Delta-Sigma A/D converter, is designed and implemented. The other interface module (encoder interface) receives the pulse signals from the incremental encoder and outputs the 12-bit position signal and 14-bit speed signal. The Avalon bus interface is the bridge for exchanging data between the NIOS II processor and the designed hardware modules. The NIOS II processor can send and receive data online. It is mainly used for debugging and monitoring the system.

The most important top level module is the designed controller. Here, it is the FOC current controller. The corresponding algorithm is divided into four reusable modules: the (*abc*-to-*dq*) and the (*dq*-to-*abc*) transformation modules, which are mainly realized by CORDIC algorithm; the anti-windup PI module; and the PWM module. The different data types of each signal in the system are clearly presented in Figure 5. Taking the u_d^*[16.4] as an example, it means that the bit width of the signal is 16, 12-bit of the integer part, and 4 bit of the fraction part.

The FPGA time/area performances of the designed FOC controller for PMSM drives are presented in Table 1 and Table 2, respectively.

Figure 6 presents the developed hardware architecture of the sensorless controller based on SMO. The design structure contains the following modules: the back EMF sliding mode observer, the CORDIC algorithm, the second order low pass filter, and the speed direction detection. In this design, the position and speed is calculated by the CORDIC algorithm. However, the calculated speed does not contain the direction information. So it

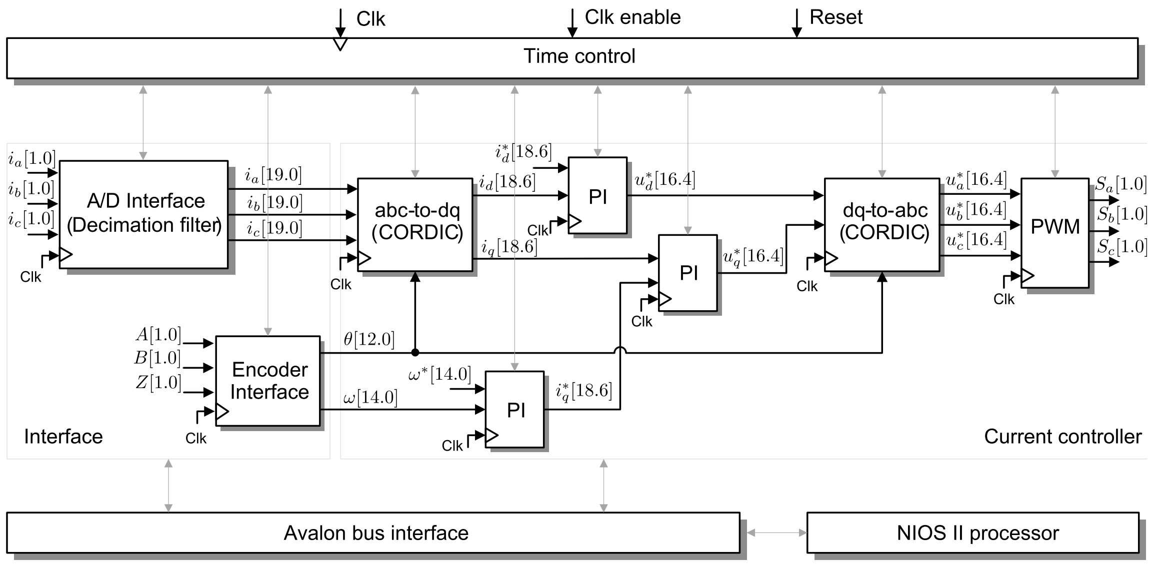

FIGURE 5. FOC FPGA implementation architecture.

TABLE 1. FPGA area utilization of FOC implementation.

EP3C40F484	Resources	Design usage
Logic elements	39600	9056 (23%)
Registers	39600	3196 (8%)
Embedded 9-bit Multiplier	252	42 (17%)

TABLE 2. FPGA time performance of FOC implementation.

Modules	Latency	Computation time
A/D interface ($Sinc3$ filter)	256	6.4 μs
Park transformation (CORDIC)	14	0.35 μs
Current PI	4	0.1 μs
Inverse Park transformation	14	0.35 μs
PWM	4	0.1 μs
Execution time	292	7.3 μs

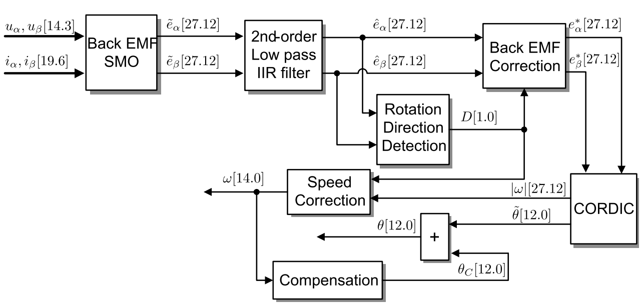

FIGURE 6. FPGA implementation hardware architecture of the sensorless controller based on SMO.

is necessary to develop a rotation direction detection algorithm.

In the industrial drive systems, the speed and position information is usually obtained from the incremental encoder. The speed direction information comes from pulse signal sequence processing. In this work, we propose a speed direction detection algorithm which is similar with that of incremental encoder. Firstly, the estimated stator frame back EMF signals are need to be processed and transformed to Boolean data types. This means that the output signal is one when the back EMF is positive. Otherwise the output signal is zero correspondingly. In addition, it is easy to see that the higher frequency the Boolean signal, the faster speed direction detection. To improve the precision, the fundamental frequency pulse signals obtained from the e_α and e_β are processed to be four times higher than the original frequency. The quadruple approach is presented in Figure 7. Signal A is the pulse signal from e_α, and signal B is from e_β. Signals A_D and B_D are both delayed signals from signals A and B, respectively. According to the logic among the four signals, the quadruple signal can be generated.

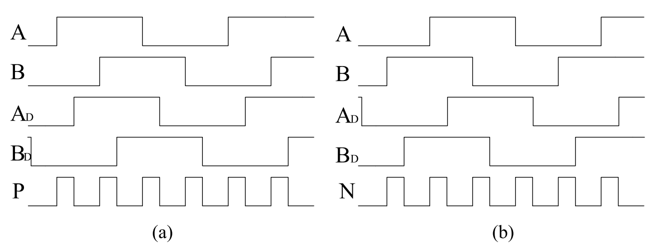

FIGURE 7. Quadruple frequency signal generation process: (a) signal A is ahead of signal B; (b) signal B is ahead of signal A.

As presented in Figure 7 (a), if A is ahead of B, the logic between the four signals and the generated quadruple signal is

$$P = A \cdot \bar{A}_D \cdot \bar{B} \cdot \bar{B}_D + A \cdot A_D \cdot B \cdot \bar{B}_D + \bar{A} \cdot A_D \cdot B \cdot B_D + \bar{A} \cdot \bar{A}_D \cdot \bar{B} \cdot B_D. \quad (32)$$

Correspondingly, when B is ahead of A, the logic is as follows

$$N = \bar{A} \cdot \bar{A}_D \cdot B \cdot \bar{B}_D + A \cdot \bar{A}_D \cdot B \cdot B_D + A \cdot A_D \cdot \bar{B} \cdot B_D + \bar{A} \cdot A_D \cdot \bar{B} \cdot B_D. \quad (33)$$

Therefore, in the situation of A ahead of B, P is the serial pulse signal when N is 0; while B is ahead of A, N is the serial pulse signal when P is 0. P and N are called quadruple positive signal and negative signal, respectively. Based on both signals of P and N, using the flip flop, the detection of rotation direction can be obtained by the following logic

$$\begin{cases} RD = \overline{N + RD1} \\ RD1 = \overline{P + RD}. \end{cases} \quad (34)$$

If the PMSM rotated at the positive direction, while there is a rising edge in P, the detection signal of the rotation direction $RD1$ is 0, and the flip-flop will hold the signal. Meanwhile, the detection signal of the rotation direction RD is 1. If the machine rotated in the negative direction, while there is a rising edge in N, RD is 0 with holding this signal by the flip-flop. Please noted that, the signal RD is the direction signal of the output rotation, i.e., $RD = 1$ refers to positive rotation; $RD = 0$ refers to negative rotation.

Table 3 presents FPGA hardware utilization of the sensorless SMO controller.

TABLE 3. FPGA area performance of the sensorless sliding mode observer.

EP3C40F484	Resources	Design usage
Logic elements	39600	3137 (8%)
Registers	39600	1135 (3%)
Embedded 9-bit Multiplier	252	180 (71%)

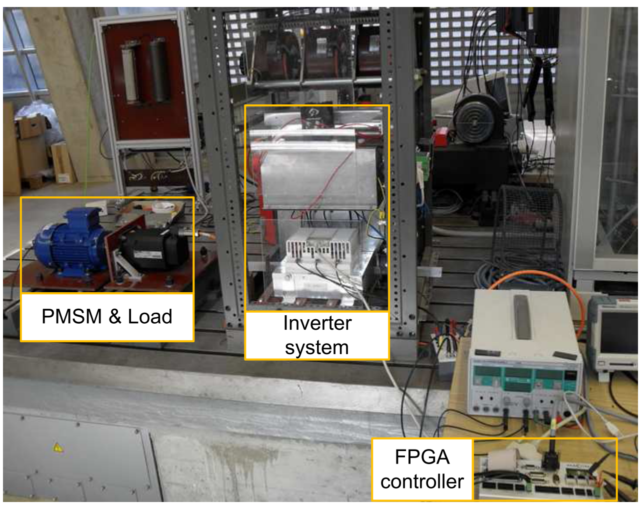

FIGURE 8. The testbench for PMSM drive systems.

TABLE 4. Nominal Parameters of SMPMSM.

Rated Power P_N	2.7 kW
Rated Torque τ_{MN}	8.5 Nm
Rated Current (eff.)	5 A
Rated Speed ω_{MN}	3000 rpm
Pole Pairs n_p	3
Rated Voltage U_N (eff.)	400 V
Stator Inductance L_s	9 mH
Stator Resistance R	1.3 Ω
PM Flux ψ_{PM}	0.41 Vs

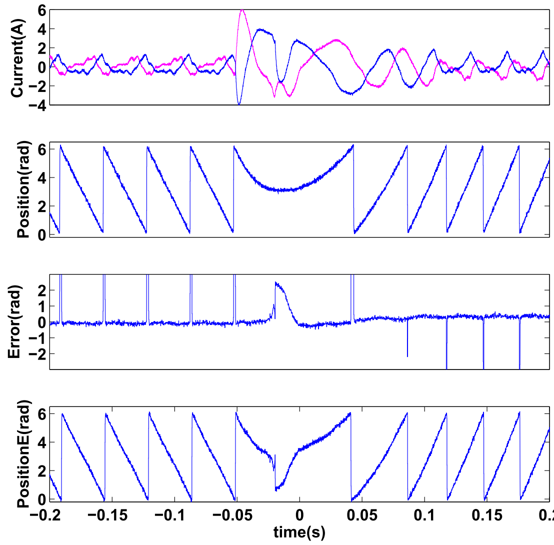

FIGURE 9. Position dynamic performance of sensorless control based on SMO from −600 rpm (0.2pu) to 800 rpm without load.

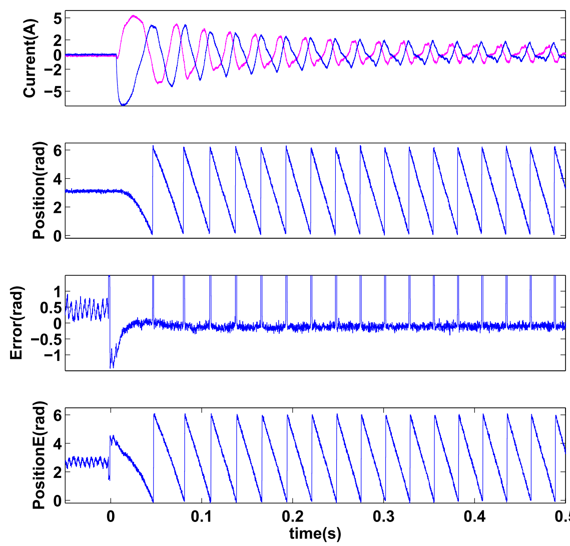

FIGURE 10. Position dynamic performance of sensorless control based on SMO with 800 rpm speed step.

V. EXPERIMENTAL RESULTS

The proposed FPGA implemented sensorless SMO together with FOC algorithm for PMSM drives was experimentally tested on a commercial 3-pole-pair SMPMSM servo motor made by Kollmorgen Seidel Corporation. The tested PMSM is fed by a two-level voltage source (VSI) inverter with a

6 kHz PWM switching frequency. The motor parameters are given in Table 4. The DC-link voltage is 300 V, the rated output voltage rms value of the inverter is 230 V. The shaft of SMPMSM is mechanically connected to an induction motor load. An incremental encoder is fixed on the shaft for obtaining actual rotor speed and position. In this work, a low cost Altera Cyclone III FPGA chip (EP3C40F484C7) is used in the control board. Figure 8 presents the whole PMSM drive experimental system with FPGA contoller.

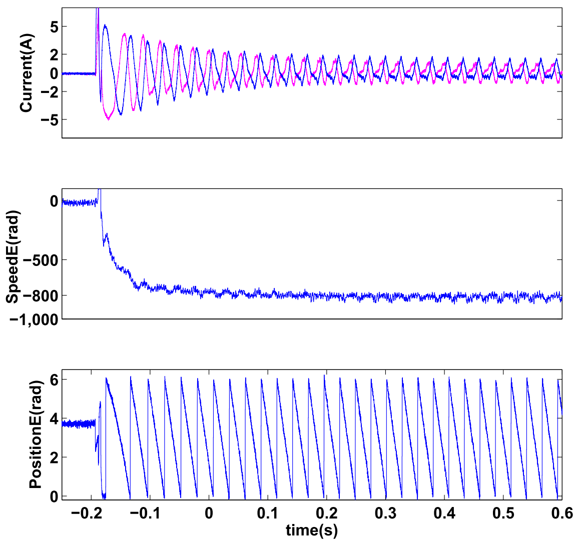

FIGURE 11. Speed dynamic performance of sensorless control based on SMO with -800 rpm speed step.

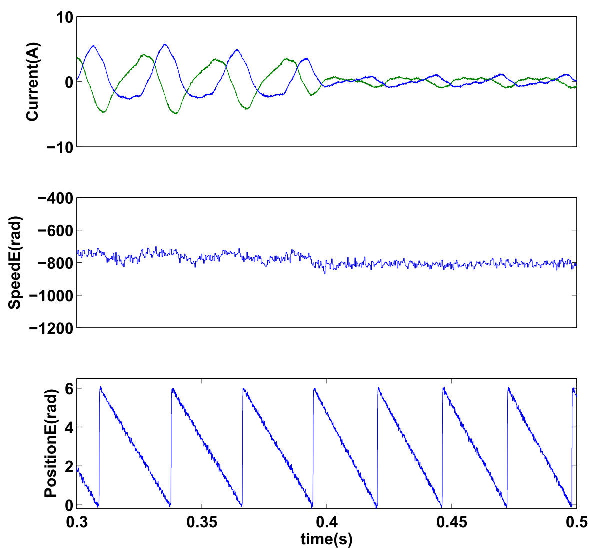

FIGURE 12. 9 Nm unload dynamic performance of sensorless control based on SMO at 800 rpm speed.

The dynamic performances of the sensorless control based on the SMO are shown in Figure 9 to Figure 12. Figure 9 presents the sensorless performance with a speed reverse from -600 rpm to 800 rpm without load. Although the estimated error is relatively large around speed of zero rpm, the transient process is very short and sensorless control can work in the whole speed range. Experimental results demonstrate that the estimated position can follow the real position tightly even though the estimated position error is relatively large at start-up and very low speed range. In Figure 10, it is shown that sensorless SMO controller can be stable even with a large speed step. Figure 11 shows the speed performance in the speed step process. With 800 rpm (0.27 pu)speed, the sensorless controller works well at the rated load, which is presented in Figure 12.

From these experimental results, we can see that the chattering problem still deteriorates the speed estimation performance (especially at low speed range) greatly even though the sign function is fully implemented on FPGA with a relative high switching frequency - 160 KHz. In conclusion, sensorless SMO is robust to parameter variation and disturbance. The robustness is unavoidablly accompanied with the chattering problem.

VI. CONCLUSION

Position and speed sensorless control algorithm for a SMPMSM using the SMO was developed and implemented in a low cost FPGA chip. In the SMO, the sliding mode manifold is chosen on the real stator current trajetory. A sign function of current error in the feedback correction is adopted. The proposed FPGA implementation architecture of FOC with sensorless SMO is elaborated in this work. CORDIC algorithm is used to calculate the estimated speed and position. In order to improve the robustness of sensorless SMO algorithm, a practice friendly speed direction detection method is proposed. The proposed rotation direction detection algorithm can detect the correct direction very fast. Therefore, it make the whole sensorless SMO much more robust compared with conventional sensorless control using SMO. Using model based design method and dedicated hardware implementation algorithms such as CORDIC, pipeline and resource sharing, the proposed sensorless controller can be implemented in relatively short execution time which improves its performance correspondingly. Experimental results present that the FPGA based sensorless controller is robust. It can work well in a wide speed range, i.e., from low speed to high speed range.

REFERENCES

[1] P. L. Jansen and R. D. Lorenz, "Transducerless position and velocity estimation in induction and salient AC machines," *IEEE Trans. Ind. Appl.*, vol. 31, no. 2, pp. 240–247, Mar. 1995.

[2] M. Linke, R. Kennel, and J. Holtz, "Sensorless position control of permanent magnet synchronous machines without limitation at zero speed," in *Proc. IECON*, vol. 1, 2002, pp. 674–679.

[3] M. J. Corley and R. D. Lorenz, "Rotor position and velocity estimation for a salient-pole permanent magnet synchronous machine at standstill and high speeds," *IEEE Trans. Ind. Appl.*, vol. 34, no. 4, pp. 784–789, Jul. 1998.

[4] E. Robeischl and M. Schroedl, "Optimized INFORM measurement sequence for sensorless PM synchronous motor drives with respect to minimum current distortion," *IEEE Trans. Ind. Appl.*, vol. 40, no. 2, pp. 591–598, Mar. 2004.

[5] Q. Gao, G. M. Asher, M. Sumner, and L. Empringham, "Position estimation of a matrix-converter-fed AC PM machine from zero to high speed using PWM excitation," *IEEE Trans. Ind. Electron.*, vol. 56, no. 6, pp. 2030–2038, Jun. 2009.

[6] R. Leidhold, "Position sensorless control of PM synchronous motors based on zero-sequence carrier injection," *IEEE Trans. Ind. Electron.*, vol. 58, no. 12, pp. 5371–5379, Dec. 2011.
[7] D. Paulus, P. Landsmann, and R. Kennel, "General arbitrary injection approach for synchronous machines," in *Proc. Symp. SLED/PRECEDE*, 2013, pp. 1–6.
[8] P. Landsmann and R. Kennel, "Saliency-based sensorless predictive torque control with reduced torque ripple," *IEEE Trans. Power Electron.*, vol. 27, no. 10, pp. 4311–4320, Oct. 2012.
[9] Z. Ma, J. Gao, and R. Kennel, "FPGA implementation of a hybrid sensorless control of SMPMSM in the whole speed range," *IEEE Trans. Ind. Informat.*, vol. 9, no. 3, pp. 1253–1261, Aug. 2013.
[10] C. Silva, G. M. Asher, and M. Sumner, "Hybrid rotor position observer for wide speed-range sensorless PM motor drives including zero speed," *IEEE Trans. Ind. Electron.*, vol. 53, no. 2, pp. 373–378, Apr. 2006.
[11] J. Hu and B. Wu, "New integration algorithms for estimating motor flux over a wide speed range," *IEEE Trans. Power Electron.*, vol. 13, no. 5, pp. 969–977, Sep. 1998.
[12] P. K. Nandam and P. C. Sen, "A comparative study of a Luenberger observer and adaptive observer-based variable structure speed control system using a self-controlled synchronous motor," *IEEE Trans. Ind. Electron.*, vol. 37, no. 2, pp. 127–132, Apr. 1990.
[13] S. Chi, Z. Zhang, and L. Xu, "Sliding-mode sensorless control of direct-drive PM synchronous motors for washing machine applications," *IEEE Trans. Ind. Appl.*, vol. 45, no. 2, pp. 582–590, Mar. 2009.
[14] M. A. M. Cheema, J. E. Fletcher, M. Farshadnia, D. Xiao, and M. F. Rahman, "Combined speed and direct thrust force control of linear permanent-magnet synchronous motors with sensorless speed estimation using a sliding-mode control with integral action," *IEEE Trans. Ind. Electron.*, vol. 64, no. 5, pp. 3489–3501, May 2017.
[15] S. Bolognani, R. Oboe, and M. Zigliotto, "Sensorless full-digital PMSM drive with EKF estimation of speed and rotor position," *IEEE Trans. Ind. Electron.*, vol. 46, no. 1, pp. 184–191, Feb. 1999.
[16] M. Rashed, P. F. A. MacConnell, A. F. Stronach, and P. Acarnley, "Sensorless indirect-rotor-field-orientation speed control of a permanent-magnet synchronous motor with stator-resistance estimation," *IEEE Trans. Ind. Electron.*, vol. 54, no. 3, pp. 1664–1675, Jun. 2007.
[17] C. Yang, T. Ma, Z. Che, and L. Zhou, "An adaptive-gain sliding mode observer for sensorless control of permanent magnet linear synchronous motors," *IEEE Access*, vol. 6, pp. 3469–3478, 2018.
[18] L. Sheng, W. Li, Y. Wang, M. Fan, and X. Yang, "Sensorless control of a shearer short-range cutting interior permanent magnet synchronous motor based on a new sliding mode observer," *IEEE Access*, vol. 5, pp. 18439–18450, 2017.
[19] L. Idkhajine, E. Monmasson, and A. Maalouf, "Fully FPGA-based sensorless control for synchronous AC drive using an extended Kalman filter," *IEEE Trans. Ind. Electron.*, vol. 59, no. 10, pp. 3908–3918, Oct. 2012.
[20] Z. Ma, S. Saeidi, and R. Kennel, "FPGA implementation of model predictive control with constant switching frequency for PMSM drives," *IEEE Trans. Ind. Informat.*, vol. 10, no. 4, pp. 2055–2063, Nov. 2014.
[21] N. K. Quang, N. T. Hieu, and Q. P. Ha, "FPGA-based sensorless PMSM speed control using reduced-order extended Kalman filters," *IEEE Trans. Ind. Electron.*, vol. 61, no. 12, pp. 6574–6582, Dec. 2014.
[22] Z. Ma, X. Zhang, J. Huang, and B. Zhao, "Stability constraining dichotomy solution based model predictive control to improve the stability of power conversion system in the MEA," *IEEE Trans. Ind. Electron.*, to be published.
[23] H. Brandtstädter, "Sliding mode control of electromechanical systems," Ph.D. dissertation, Inst. Autom. Control Eng., Tech. Univ. Munich, Munich, Germany, 2009.
[24] L. Zhang, Y. Fan, C. Li, A. Nied, and M. Cheng, "Fault-tolerant sensorless control of a five-phase FTFSCW-IPM motor based on a wide-speed strong-robustness sliding mode observer," *IEEE Trans. Energy Convers.*, vol. 33, no. 1, pp. 87–95, Mar. 2018.

ZHIXUN MA (S'13–M'15) received the B.S. and M.S. degrees in electrical engineering from the China University of Mining and Technology, Xuzhou, China, in 2006 and 2009, respectively, and the Ph.D. degree in electrical engineering from the Technical University of Munich, Germany, in 2014. He is currently an Associate Professor with the National Maglev Transportation Engineering R&D Center, Tongji University, Shanghai, China. He is also a Research Fellow with Nanyang Technological University, Singapore. His main research areas include predictive control and sensorless control of electrical drives, renewable energy systems, and FPGA-based digital control of power electronics and drive systems.

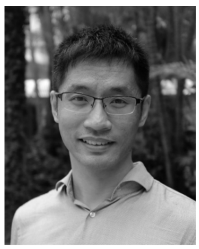

XIN ZHANG (M'15) received the Ph.D. degree in automatic control and systems engineering from The University of Sheffield, U.K., in 2016, and the Ph.D. degree in electronic and electrical engineering from the Nanjing University of Aeronautics and Astronautics, China, in 2014. He was a Post-Doctoral Research Fellow with the City University of Hong Kong in 2017 and a Research Associate with The University of Sheffield from 2014 to 2016. He is currently an Assistant Professor of power engineering with the School of Electrical and Electronic Engineering, Nanyang Technological University. He is generally interested in power electronics, power system, and advanced control theory, together with their applications in various sectors. He received the highly prestigious Chinese National Award for Outstanding Students Abroad in 2016.